JACS
JOURNAL OF THE AMERICAN CHEMICAL SOCIETY

Article

pubs.acs.org/JACS

Emergence of Function in P450-Proteins: A Combined Quantum Mechanical/Molecular Mechanical and Molecular Dynamics Study of the Reactive Species in the H_2O_2-Dependent Cytochrome $P450_{SP\alpha}$ and Its Regio- and Enantioselective Hydroxylation of Fatty Acids

Rajeev Ramanan, Kshatresh Dutta Dubey, Binju Wang, Debasish Mandal, and Sason Shaik*

Institute of Chemistry and the Lise Meitner-Minerva Center for Computational Quantum Chemistry, The Hebrew University of Jerusalem, 91904 Jerusalem, Israel

Supporting Information

ABSTRACT: This work uses combined quantum mechanical/molecular mechanical and molecular dynamics simulations to investigate the mechanism and selectivity of H_2O_2-dependent hydroxylation of fatty acids by the $P450_{SP\alpha}$ class of enzymes. H_2O_2 is found to serve as the surrogate oxidant for generating the principal oxidant, Compound I (Cpd I), in a mechanism that involves homolytic O−O bond cleavage followed by H-abstraction from the Fe−OH moiety. Our results rule out a substrate-assisted heterolytic cleavage of H_2O_2 en route to Cpd I. We show, however, that substrate binding stabilizes the resultant Fe−H_2O_2 complex, which is crucial for the formation of Cpd I in the homolytic pathway. *A network of hydrogen bonds locks the HO· radical*, formed by the O−O homolysis, thus directing it to exclusively abstract the hydrogen atom from Fe−OH, thereby forming Cpd I, while preventing the autoxoidative reaction, with the porphyrin ligand, and the substrate oxidation. The so formed Cpd I subsequently hydroxylates fatty acids at their α-position with *S*-enantioselectivity. These selectivity patterns are controlled by the active site: substrate's binding by Arg241 determines the α-regioselectivity, while the Pro242 residue locks the prochiral α-CH_2, thereby leading to hydroxylation of the *pro-S* C−H bond. Our study of the mutant Pro242Ala sheds light on potential modifications of the enzyme's active site in order to modify reaction selectivity. Comparisons of $P450_{SP\alpha}$ to $P450_{BM3}$ and to $P450_{BS\beta}$ reveal that *function* has evolved *in these related metalloenzymes by strategically placing very few residues in the active site.*

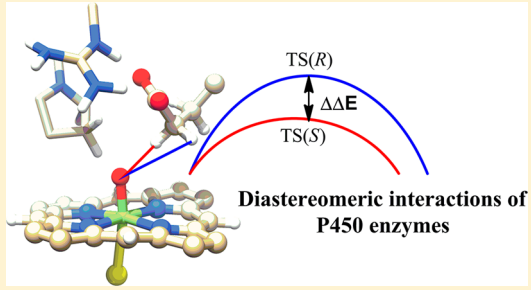

1. INTRODUCTION

The cytochrome P450 class of enzymes catalyzes a wide range of reactions such as hydroxylation, epoxidation, reductive dehalogenation, amine dealkylation and sulfoxidations.[1] The coupled high-valent iron(IV)−oxoporphyrin π−cation radical, so-called compound I (Cpd I), is the reactive intermediate that performs all these reactions, once it is formed in the catalytic cycle of P450s. The native process for Cpd I formation involves reductive activation of molecular oxygen, by NADPH or NADH, followed by double protonation on the distal oxygen and departure of a water molecule.[1] Alternatively, Cpd I can be generated from a ferric hydrogen peroxide ($Fe^{III}(O_2H_2)$) complex (or other peroxides), by shunting the native cycle.[1,2] This latter mode of generating Cpd I could have been in principle very efficient, since the catalytic system is no more dependent on electron donating cofactors, such as NADPH or NADH, which slow down the catalytic cycle.[1] However, in practice, shunting is generally less common for native enzymes that use reducing cofactors.

In 1994, Matsunaga et al.[3] made an important discovery of the first H_2O_2-dependent P450 enzyme, which was isolated from *Sphingomonas paucimobilis*.[3] Matsunaga et al., further reported that this P450 performs the hydroxylation of long chain fatty acids in an α-regioselective manner (α- is the CH_2 position adjacent to the carboxylate; see Scheme 1b), and was hence called $P450_{SP\alpha}$ (or CYP152B1 in the systematic nomenclature).[4a] The authors corroborated the H_2O_2 dependency of enzyme in line with a previous report on fat metabolism in plants where an H_2O_2 generating system was a prerequisite for the α oxidation.[4b] This regioselectivity can be contrasted with that of $P450_{BM3}$, which hydroxylates fatty acids at the CH_2 groups ω-1/ω-2/ω-3 in the hydrophobic tail.[5] It is also different than the β regioselectivity found for the closely related $P450_{BS\beta}$ enzyme.[6] How do these three related hydroxylases acquire different functions? This is an interesting question, which is pondered in this work.

In 2003, the first crystal structure of another H_2O_2-dependent $P450_{BS\beta}$ was reported by Lee et al.,[6] and was found to catalyze the hydroxylation of fatty acids dominantly at the β position.[6] This crystal structure revealed that the distal pair of acid−base residues that are crucial for Cpd I formation in the "normal" catalytic cycle were absent in this H_2O_2-dependent $P450_{BS\beta}$ enzyme.[6] Furthermore, unlike in $P450_{BM3}$

Received: February 16, 2016
Published: April 8, 2016

DOI: 10.1021/jacs.6b01716
J. Am. Chem. Soc. 2016, 138, 6786−6797

Scheme 1[a]

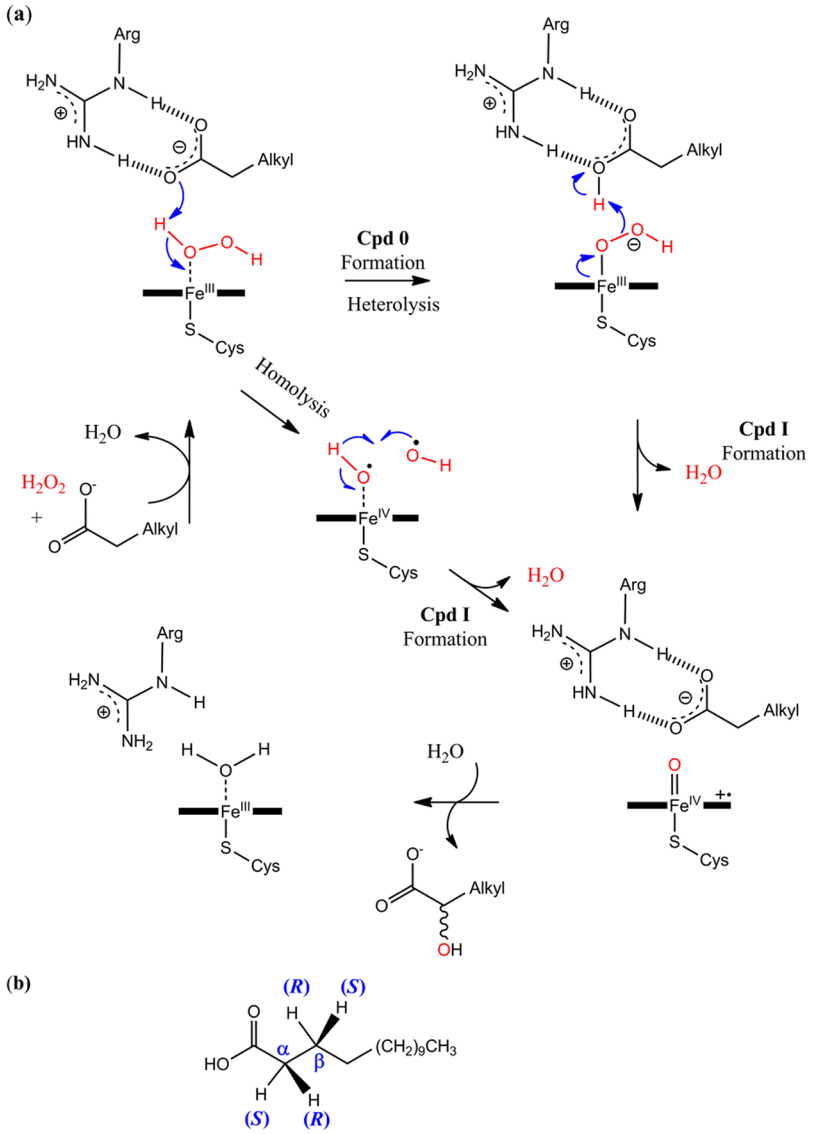

[a](a) A mechanistic scheme of substrate-assisted catalysis and homolytically-initiated pathways in $P450_{SP\alpha}$, a hydroxylase of fatty acids. (b) A fatty acid with indications of its α and β positions, and the corresponding *pro-R* and *pro-S* C−H bonds.

where the fatty acid is bound by its carboxylic head near the protein surface, here in $P450_{BS\beta}$ the carboxylate head goes deep into the distal side of the heme where it gets bound by Arg242. It was proposed,[6] that the amino acid residue Arg242 teams with the carboxylate of the fatty-acid substrate, which together constitute the requisite acid−base pair needed for heterolytic O−O cleavage and generation of Cpd I, as depicted in Scheme 1a. The proposal of substrate-assisted catalysis was tested using a related H_2O_2-dependent enzyme, $P450_{BS\beta}$ (CYP152A1) enzyme, which could hydroxylate styrene and ethylbenzene in the presence of carboxylic acid with short side chain,[7] but failed to do so in the absence of the carboxylic acid. These reports seemed to confirm the crucial role of carboxylate binding in substrate oxidations.

Subsequently, in 2011, Fujishiro et al.[8] reported the H_2O_2-dependent hydroxylation of myristic acid, $CH_3(CH_2)_{12}COOH$, by the $P450_{SP\alpha}$ enzyme with high α-regio- and *S*-stereoselectivities (see Scheme 1). They also reported the selectivity of two mutants along with wild type, and showed that the regio- and stereoselectivity can go up to >99% and 97%, respectively.

Summing all the above information, $P450_{SP\alpha}$ has a few intriguing features: (a) the enzyme seems to possess a novel substrate-dependent mechanism of Cpd I formation via Cpd 0, and (b) its hydroxylation activity is highly selective for the α-position and for the *pro-S* C−H bond. Does Cpd I formation in this H_2O_2-dependent enzyme proceed via Cpd 0? What are the factors that control these selective modes of hydroxylation? And why are these modes of $P450_{SP\alpha}$ so different compared with the $P450_{BM3}$ and $P450_{BS\beta}$ enzymes? These issues form the focus of the present paper, which seeks detailed atomistic insight into the emergence of function using QM/MM calculations and MD simulations.

The first issue concerns the mechanism of Cpd I formation. Starting from an $Fe^{III}(O_2H_2)$ complex, the O−O bond can either undergo homolytic or heterolytic cleavages. Homolytic cleavage in the active site of a P450 enzyme, is generally viewed with skepticism since it "liberates" hydroxyl radicals,[9] which

DOI: 10.1021/jacs.6b01716
J. Am. Chem. Soc. 2016, 138, 6786−6797

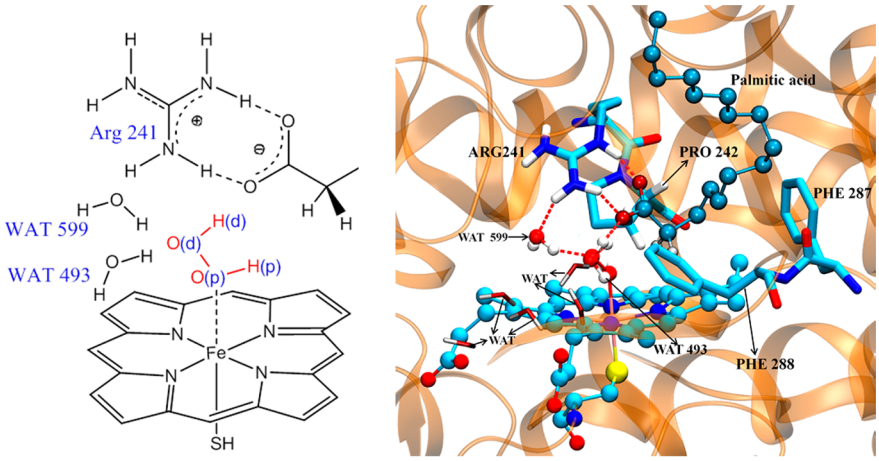

(a) (b)

Figure 1. (a) Schematic representation of the QM region used in the study. (b) An MD snapshot showing the QM system inside the enzyme cavity, with marking of the H-bonds, and key residues (e.g., Phe288, Arg241 and Pro242).

may destroy the enzymatic activity. The common wisdom is that P450s evolved by nature to ensure the dominance of the heterolytic pathway. Heterolytic cleavage begins with the formation of Cpd 0 in the catalytic cycle.[1] A basic residue near the active site can abstract the proximal proton from the $Fe^{III}(O_2H_2)$ complex. This step is followed by a heterolytic cleavage of the O−O bond which eventually leads to the formation of the Cpd I. However, this generally accepted proposal has also some exceptions with cases where Cpd 0 is bypassed.[10] Thus, Sicking et al. showed that O−O homolysis of a $Fe^{III}(O_2H_2)$ complex leads to the formation of Cpd I.[11] Subsequently, this mechanism was found to be quite facile in Nitric oxide synthase[10a] and more recently in $P450_{CAM}$ and its T252A mutant.[10c] In all these cases, the O−O homolysis is followed by selective and very fast hydrogen atom abstraction (H-abstraction) from the Fe(IV)−OH by the nascent HO· radical, which is held and directed by a net of H-bonds with the surrounding protein. We shall therefore test the two alternative hypotheses for Cpd I, as depicted in Scheme 1: the O−O homolysis/H-abstraction mechanism vs the heterolytic mechanism, whereby the carboxylic group of the substrate could trigger acid−base catalytic function. The selectivity issues may derive from constraints in the binding channel of the substrate, and would require an atomistic calculation within the native protein.

To study all these issues we use combined quantum mechanical/molecular mechanical (QM/MM) and molecular dynamics (MD) simulations. As such, we elucidate a detailed mechanism of the Cpd I formation from the $Fe^{III}(O_2H_2)$ complex, and unravel the preferable interactions within the active site, which cause this feat of selectivity. As we demonstrate, the mechanism of Cpd I formation involves homolytic O−O cleavage followed by selective and exclusive hydrogen abstraction from the Fe(IV)−OH by the nascent HO· radical, as demonstrated in recent studies.[10a,c] Furthermore, we show that the substrate binding by Arg241 and with assistance from Phe288 bring about the α-CH_2 regioselectivity, while Pro242 and the enzyme's cavity apply *diastereomeric interactions* which lead to *S*-hydroxylaton at the α-CH_2 position. This will be followed by comparison of the different functions of the three related enzymes: $P450_{SP\alpha}$, $P450_{BS\beta}$, and $P450_{BM3}$.

2. COMPUTATIONAL METHODS AND DETAILS

2.1. System Setup. The initial structure of the enzyme was taken from the X-ray structure of the CYP152B1 with palmitic acid, $CH_3(CH_2)_{14}COOH$, as substrate (PDB code 3AWM).[8] The crystal structure has a resolution of 1.65 Å. For determination of the protonation state of residues, the pK_a values of amino acid residues were calculated with PROPKA software.[12] The protonation states of the histidine residues were assigned based on the pK_a values and the neighboring structures for possible hydrogen bonds. On the basis of such judgments, the histidine residues 91, 93, 230, 255, 321, 355, 359, 376, and 412 are protonated at the ε position (HSE) while 138, 179, 219, and 223 are protonated at the δ position (HSD). The resulting protein had a 4^- charge, which based on previous experience does not make much of a difference in the final QM/MM results (a recent report from our lab, which showed that an enzyme with a charge 8^- and the corresponding neutralized one have little effect on Fe(O−O) bond homolysis in $Fe^{III}(O_2H_2)$ complex[10c]).

2.2. MD Simulation. The crystal structure had an axial water molecule coordinated to Fe^{III}. This water molecule was modified to model the structures of both Cpd I and $Fe^{III}(O_2H_2)$ complex. A water layer of 16 Å from protein exterior was added with TIP3P[13] water model using solvate package of VMD.[14] For the purposes of preparing the QM/MM calculation runs,[15] we initially followed the standardized procedure for protein solvation using non periodic simulations, as suggested by Thiel and co-workers.[15a,b] Minimization was performed in two steps; first keeping the protein fixed and then a whole system minimization without any restraints using 5000 steps of conjugate gradient algorithm, to remove any of the steric clashes during system setup. Thereafter, equilibration dynamics was performed using Langevin dynamics[16] with damping coefficient of 1 ps^{-1}, which was preceded by system annealing at the target temperature of 300 K. All simulations were performed in nonperiodic boundary conditions using spherical boundary and switching potential function with a cutoff of 12 Å. We used CHARMM22 force field for protein and solvation[17] and previously published force field for Fe-(O_2H_2) fragment.[18] We continued 25 ns of production dynamics for Cpd I and 10 ns for $Fe^{III}(O_2H_2)$ complex using the same system setup and MD procedure. All MD simulations were carried out with NAMD software package.[19]

2.3. QM/MM Methodology. All QM/MM calculations were performed with ChemShell software.[20] Turbomole[21] was used for the QM region and DL_POLY[22] for the MM part. The polarizing effect of the enzyme on the QM region was accounted by the electronic embedding scheme.[23] As shown in Figure 1, we included in the QM region the following molecules and protein residues: the truncated heme unit, the carboxyl end of the fatty acid with the α and β carbon atoms, the guanidinium end of Arg241 and the two crystal water molecules. Since the heme unit was carved from the enzyme at the

DOI: 10.1021/jacs.6b01716
J. Am. Chem. Soc. 2016, 138, 6786−6797

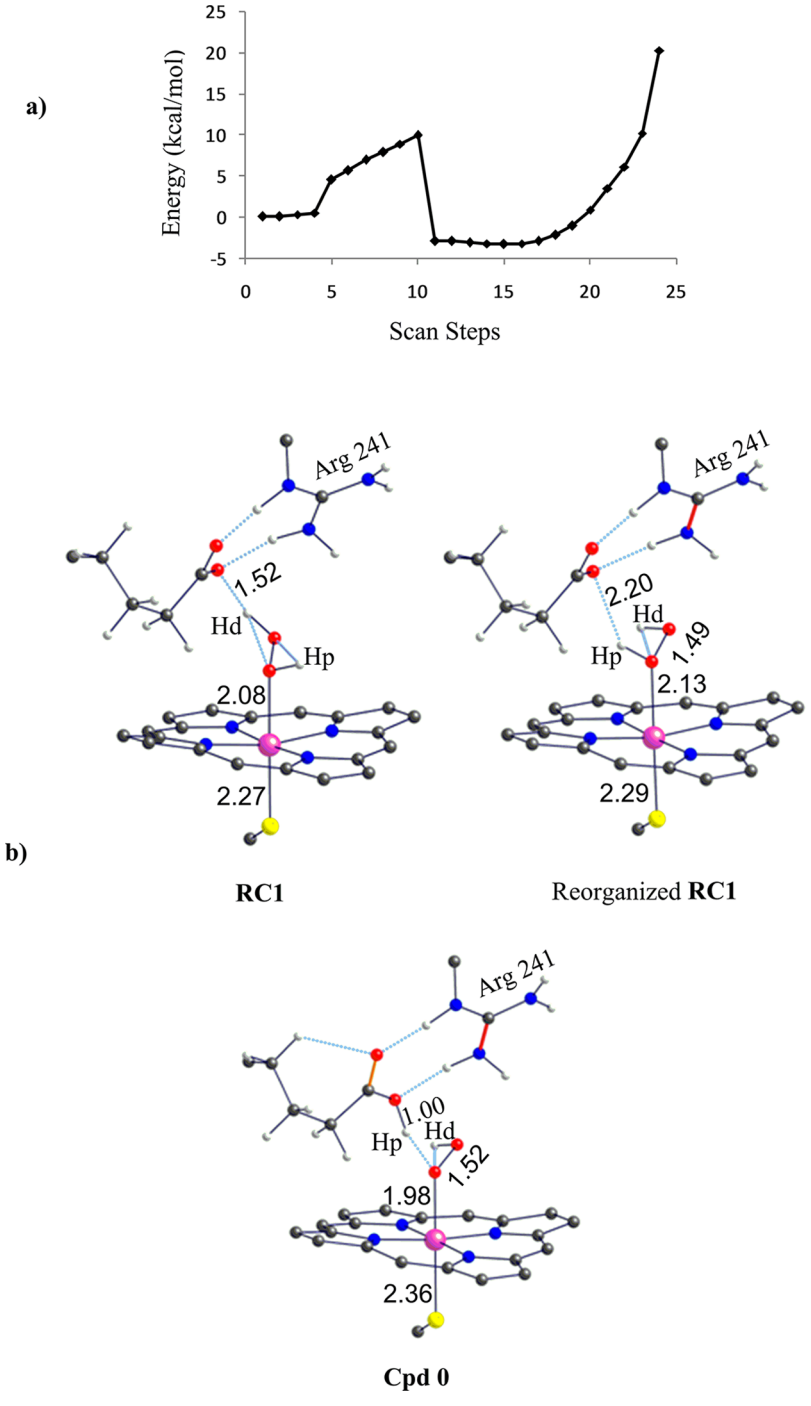

Figure 2. (a) The scanned energy profile for Cpd 0's formation from $Fe^{III}(O_2H_2)$ at the QM(B1)/MM level of theory. (b) Geometries of $Fe^{III}(O_2H_2)$, denoted as **RC1**, and **Cpd 0**.

sulfur of the cysteinate ligand, we used a hydrogen link atom with charge shift model,[20] for the QM/MM boundary.

Unrestricted B3LYP functional was used for the QM calculations.[24] It was reported that UB3LYP functional shows better accuracy, compared with a variety of other functionals, for an Fe-oxo system in hydrogen abstraction reactions.[25] For geometry optimization we employed a basis set, so-called B1, consisting of 6-31G* for sulfur, LACVP for iron and 6-31G for all other atoms.[26] Single point energies were calculated at the more extended basis set, def2-TZVP, which is labeled as B2.[27]

Transition state (TS) optimizations were carried out in two steps. First, a relaxed potential energy scan was performed along the reaction coordinate with a step size of 0.1 Å, going from reactants to products. The highest energy point on this potential energy surface (PES) was further optimized without any constraints using P-RFO optimizer in the HDLC code.[28] Frequency calculations of all optimized geometries were used to ensure that the minima and transition states are genuine. Optimized reactants and products were devoid of any imaginary frequencies. All the transition states showed single imaginary frequency except for the one for *meso* hydroxylation (vide infra), which was difficult to characterize, as it did not show any imaginary frequency. To verify it as the genuine highest energy point, the relaxed potential energy scan was repeated by steps of 0.02 Å units.[29] These entire scan profiles are given in Figure S1 of Supporting Information (SI). The lowest energy difference between any of the two competitive

DOI: 10.1021/jacs.6b01716
J. Am. Chem. Soc. 2016, 138, 6786−6797

Scheme 2. Potential Reaction Pathways after the Homolysis of $Fe^{III}(O_2H_2)$ Complex

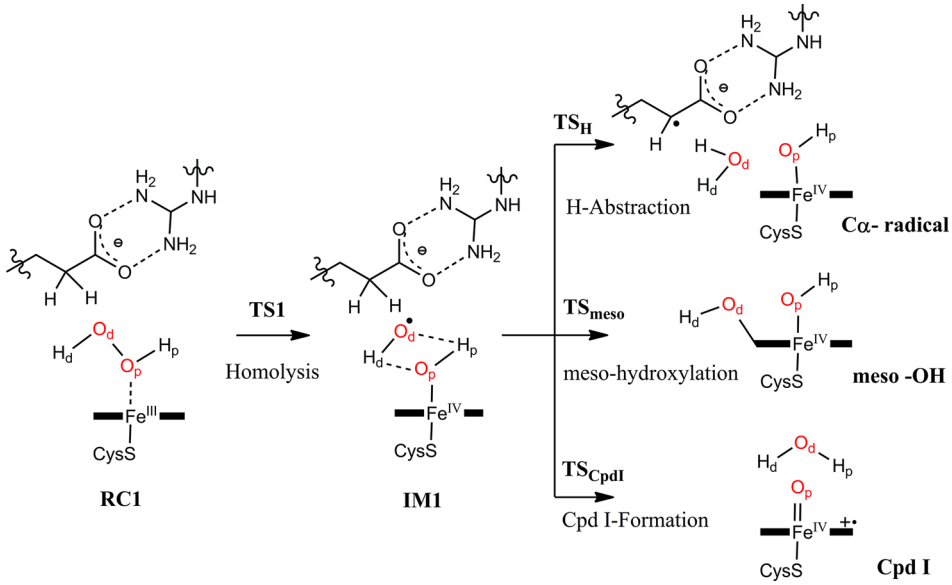

pathways in the following discussions is more than 6 kcal/mol. So the methods applied here are robust enough to handle the present study.

Gaussian 09 was used to perform single point calculations[30] for analysis of the distortion and interaction energies in the transition states.[31,32] To determine these quantities we calculated the QM system embedded in a solvent having approximately the dielectric constant of a nonpolar protein (diethyl ether, $\varepsilon = 4.24$). Details of this method are given in the Supporting Information (SI) document (page S9).

Reactive spin states for Cpd I and $Fe^{III}(O_2H_2)$ involve the doublet spin states (S = 1/2).[33] Details of the ground state and reactive spin states of $Fe^{III}(O_2H_2)$ complex were reported in a QM-only study and in protein environment by QM/MM studies.[10c,33] The ground state for $Fe^{III}(O_2H_2)$ is the sextet state (S = 5/2), followed by the quartet state (S = 3/2) and the doublet state. However, since the doublet state is the only bound state, and it also has the smallest barrier for O−O bond homolysis,[10c,33] we used this state throughout the study. The sextet and quartet states have a long Fe−O distance, and hence are thought to lead to H_2O_2 liberation in P450.[10c] However, for this H_2O_2–dependent enzyme, the H_2O_2 liberation is obviously irrelevant, as the H_2O_2 is held by H-bonding in a tight space among the substrate, heme and the enzyme surroundings (see Figure 1b and the discussion of the MD simulation in the following section). These surroundings can barricade the liberation of H_2O_2.

3. RESULTS AND DISCUSSIONS

The catalytic cycle of the reaction starts with the formation of the $Fe^{III}(O_2H_2)$ complex. The MD study showed that the $Fe^{III}(O_2H_2)$ complex is indeed a stable intermediate, such that during the entire simulation of 10 ns H_2O_2 never departed from the heme unit. Similar stable Fe-(O_2H_2) complexes are reported in our previous study on Horseradish peroxidase enzymes also.[34] Indeed, as we mentioned above, the H_2O_2 molecule so coordinated to Fe is stabilized by hydrogen bonding with the carboxylate group of fatty acid, and the barricades raised by the active site surroundings. The distal proton, H_d, (Figure 1) makes a hydrogen bond with the carboxyl group of the fatty acid. This hydrogen bonding is found to be stable during the entire simulation time. The distance of this hydrogen bonding is shown in Figure S2 of the SI document along with the Fe−O distance for the entire simulation of 10 ns. The distance of the proximal O−H_p (Figure 1a) proton from the carboxyl group is always long during the dynamics. Water molecules are consistently present in the distal pocket of the heme and these molecules further stabilize the complex through hydrogen bonding. The salt bridge between Arg241 and the carboxylate group of substrate is also found to be stable. This salt bridge holds the substrate tightly in the active site. Also, the coordination of H_2O_2 does not affect the conformation of the substrate fatty acid molecule. Figure 1b shows a proper representation of the crucial hydrogen bonds, salt bridge, orientation of H_2O_2 and the conformation of fatty acid substrate at the active site of enzyme.

3.1. Formation of Cpd 0 via a Substrate Assisted Mechanism. Generally, Cpd 0's formation is considered as the prerequisite for the eventual formation of Cpd I.[1] Abstraction of the proximal proton, H_p (Figure 1a), of H_2O_2 by the substrate's carboxylate could in principle generate Cpd 0. The potential energy surface for the proton abstraction, obtained by a scan from the $Fe^{III}(O_2H_2)$ complex (**RC1**), is shown in Figure 2, and is seen to require two steps and a high energy expense. The first step in Figure 2, involves H-bonding reorganization. Thus, throughout the dynamics of the substrate inside the active site, it is the distal proton, H_d, that maintains H-bonding with the carboxylate group of fatty acid, while Cpd 0 formation requires abstraction of the proximal proton, H_p, by the carboxyl group. Therefore, juxtaposing the carboxylate and H_p requires reorganizing the $Fe^{III}(O_2H_2)$ complex to a conformation that is prepared for the ensuing proton abstraction of H_p. An upper limit for this reorganization energy was found to be 9.8 kcal/mol at the QM(B1)/MM level of theory. Subsequently, proton transfer can transpire, but at the point where the carboxylic OH distance became 0.901 Å, the formation of COOH turned out to be highly endothermic by 20.2 kcal/mol. The reason for this endothermicity is the disruption of the salt bridge between Arg241 with the carboxylate group, which attends Cpd 0 formation. As such, this highly endothermic formation of Cpd 0 is ruled out as a feasible process for the enzyme. Additionally, because of this endothermicity, all our attempts to optimize the carboxylic acid product always resulted back in the formation of $Fe^{III}(O_2H_2)$ complex. A similar finding was reported in an earlier study also,[10a] where Cpd 0 formation was found to be endothermic of the amount 15.0 kcal/mol.

DOI: 10.1021/jacs.6b01716
J. Am. Chem. Soc. 2016, 138, 6786−6797

3.2. Cpd I Formation through the O−O Bond Homolysis/H-Abstraction Mechanism. Since formation of Cpd 0 has been reasonably ruled out above, we turn here to consider the alternative mechanistic hypothesis. As shown in Scheme 2 (see corresponding electronic structures and spin density data in Figure S3 and Table S1 to S4 in the SI document), this mechanism commences with the homolysis of the O−O to form the **IM1** intermediate, which involves a HO· radical bound to Fe(IV)−OH complex, and thereafter the intermediate can in principle participate in three competing follow-up reactions: H-abstraction from the substrate by the HO· radical, attack of the HO· radical on the *meso* carbon of the porphyrin ligand, and Cpd I formation by H-abstraction from Fe(IV)−OH. Note that the *meso* hydroxylation of the porphyrin ligand is a well-known heme degradation pathway,[9b] while H-abstraction from the substrate represents the direct oxidative pathway by H_2O_2.

Figure 3 shows the energy profiles corresponding to these mechanistic pathways, while Figures 4 and 5 show the geometries of **RC1**, **TS1** and **IM1** and the **TSs** for the follow-up reactions of the intermediate. As seen from Figure 3, the O−O bond homolysis has a low barrier of 10.9 kcal/mol (including ZPE correction), leading to the low-energy intermediate **IM1**, which undergoes follow up reactions. Among these reactions the most facile by far is the formation of Cpd I. The *meso* attack and H-abstraction from the substrate have much higher barriers. *It is very clear therefore that P450$_{SPα}$ enzyme evolved to steer the Fe^{III}(O_2H_2) complex directly to the formation of Cpd I, without any side reactions.*

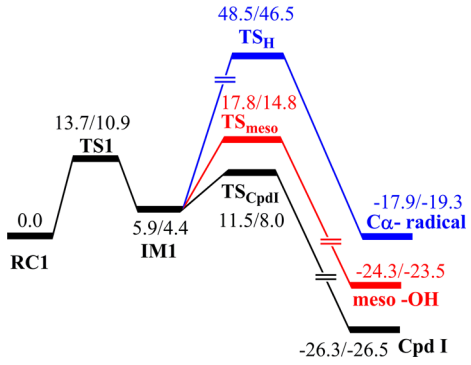

Figure 3. Potential energy profile of the homolysis of Fe^{III}(O_2H_2) complex. Energies (in kcal/mol) are represented as QM(B2)/MM followed by QM(B2+ZPE)/MM levels of theory.

Figure 4 provides some clues for the specifically targeted pathway of the Fe^{III}(O_2H_2) complex. Thus, inspection of **IM1** reveals that the carboxylate head of the substrate and the Arg241-crystal-water moiety hold the HO· radical tightly, thereby orienting its radical end (on the O) toward the H−O bond of Fe(IV)−OH. This orientation is further visible in **TS1**, which is highly stabilized by these H-bonds. Apart from these hydrogen bonds, the surrounding water networks as shown in Figure 1b at the active site ensure continued proximity of water molecule and as such, a significant stabilization of **IM1**. This highlights the importance of the substrate and surrounding water molecules. In fact, in the O_2-dependent P450s too, the hydrogen bonding network of surrounding water molecules provide a proton relay channel that is crucial for activating the O−O bond of O_2, thus leading to Cpd I generation.[10c]

The geometrical features of **IM1** reveal minute changes in comparison to **TS1**. The O−O bond distance increased from 1.83 to 2.18 Å. Intramolecular hydrogen bonds are intact as evidenced by the hydrogen bond distances, O_d−H_p and, O_p−H_d which are respectively 2.37 and 2.17 Å. Because of this arsenal of H-bonds, the intermediate **IM1** that is formed by an intrinsically endothermic O−O bond breakage nevertheless lies only at 4.4 kcal/mol relative to **RC1** as shown in Figure 3. Thus, the substrate's carboxylic head plays a role in catalyzing Cpd I formation, but this is expressed via the homolytic breakage of O−O bond in Fe^{III}(O_2H_2).

The H-bonding machinery controls also the selectivity of the **IM1** intermediate by raising the energies of the TSs in the disfavored follow-up reactions, while lowering it for the favored one. This is reflected also in the corresponding transition state geometries in Figure 5. Thus, **TS$_{CpdI}$** is quite and close to **IM1**; the Fe−O bond distance is still long, the Fe−S distance is short (2.37 Å) and the O_p−H_p is still short, while the H-bond network is largely intact. Furthermore, Cpd I is thermodynamically favored as noted by the exothermicity of −26.5 kcal/mol, which makes reaction irreversible. *All these factors ensure an efficient formation of Cpd I, thus creating function for the enzyme.*

The **TS$_{meso}$** species involves deformation of the heme, but most of its distortive features reflect the need to release the radical from the clutches of the H-bonding machinery and bring it to a bond making distance to the *meso* carbon. These changes are reflected in the much higher barrier of 14.8 kcal/mol, at the

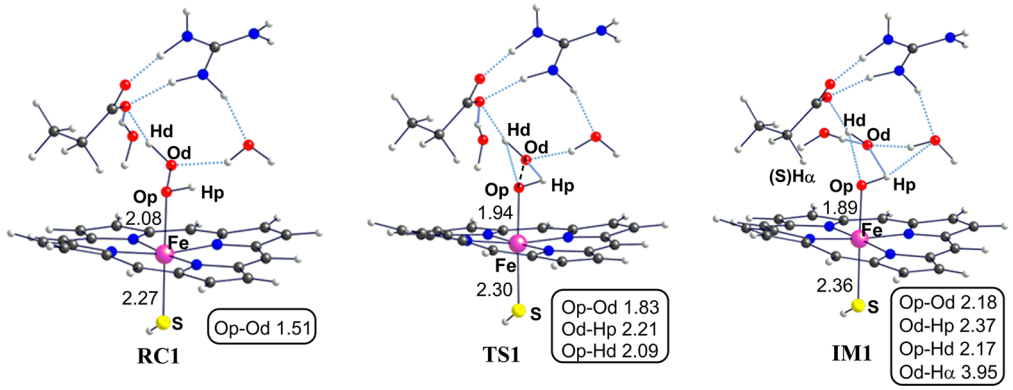

Figure 4. Optimized geometries of species involved in the O−O bond homolysis of Fe^{III}(O_2H_2) complex at the QM(B1)/MM level of theory. Distances are given in Å.

DOI: 10.1021/jacs.6b01716
J. Am. Chem. Soc. 2016, 138, 6786−6797

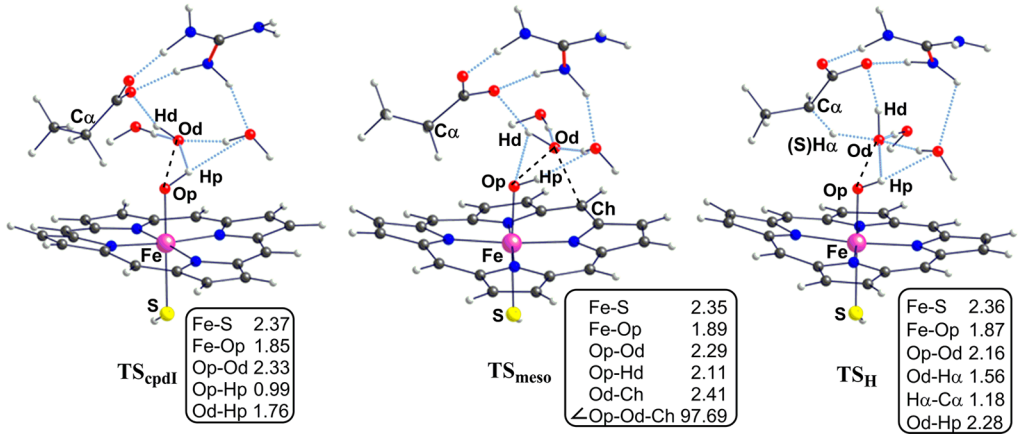

Figure 5. Optimized transition state geometries of Cpd I formation and its competitive pathways at the QM(B1)/MM level of theory. Distances are given in Å and angles are in degrees.

Scheme 3. General Mechanism of Hydroxylation of Substrates by Cpd I[a]

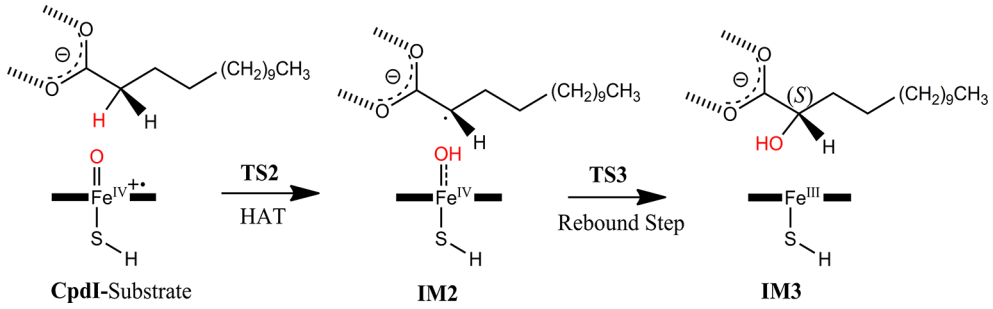

[a]The red H is *pro-S*.

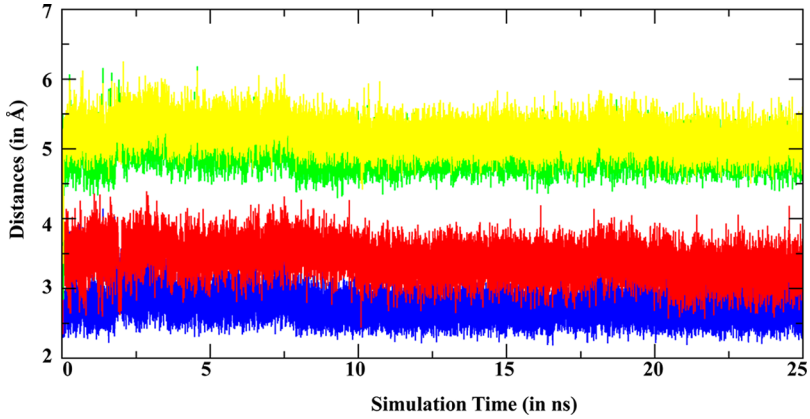

Figure 6. H−O distances of the prochiral hydrogen atoms from the oxo ligand of Cpd I during simulation of 25 ns. Color codes are blue-α (S) and red-α (R) prochiral hydrogen atoms, yellow and green are the β hydrogen atoms.

QM(B2+ZPE)/MM level, for *meso* hydroxylation vs. Cpd I formation.

Finally, the α-hydrogen abstraction needs more geometric rearrangements, since the *pro-S* hydrogen atom at the Cα of fatty acid are 3.95 Å away from distal oxygen at the optimized geometry of **IM1**. At the transition state this distance is reduced to 1.56 Å. This shortening could disrupt the water network and force the substrate to change its position. All these interactions with the enzyme get disrupted during the relocation of the substrate. The cumulative effects of all these factors increase the barrier of hydrogen atom abstraction, such that Fe^{III}(O_2H_2) plays no direct role in hydroxylation. Geometries of all these products are given in Figure S4 in SI document.

3.3. Regio- and Stereoselective Hydroxylation by Cpd I.

Let us discuss the regio- and stereoselectivity of hydroxylation by Cpd I. These selectivity features may originate from substrate dynamics as well as from *diastereomeric interactions* within the active site, which together cause the α-C−H to be closer to Cpd I (than β-C−H) while at the same time juxtaposing the prochiral α-C−H vis-à-vis Cpd I. A detailed explanation of how the substrate binding and architecture of the active site lead to observed regio/stereoselectivity follows.

DOI: 10.1021/jacs.6b01716
J. Am. Chem. Soc. 2016, 138, 6786−6797

A generic mechanism of hydroxylation by Cpd I is depicted in Scheme 3. The first step involves a hydrogen atom transfer (HAT) from the α-CH_2 group to the Fe-oxo moiety of Cpd I. Subsequently, HAT is followed by the rebound step that transfers the hydroxyl group from Fe to the α carbon radical and yields the hydroxylated product. The resultant enantioselectivity of hydroxylation will be determined by the accessibility of a given prochiral hydrogen atom to the Fe-oxo moiety. Since the carboxyl head of the substrate is tightly bonded via its H-bonds/salt bridges, the resultant α carbon radical can not flip its configuration, such that stereoselectivity is determined by the juxtaposition of one of the prochiral hydrogens. Consequently, the HAT step is expected to be the selectivity-determining step.

Figure 6 shows the distance fluctuations between the oxygen ligand of Cpd I and the four prochiral hydrogen atoms, α-*R*, α-*S*, β-*R* and β-*S*, of the fatty acid over the course of the 25 ns of dynamics. The prochiral α-*S* hydrogen atom was found to be invariably the closest one to the Fe-oxo (see the blue MD distance fluctuations in Figure 6).

To understand the relative proximities of the four hydrogens to the oxo ligand in Figure 6, we can first compare the positioning of the α and β carbons and subsequently those of the α-*R* and α-*S* hydrogen atoms. Thus, during the entire duration of the 25 ns of dynamics, the substrate did not exhibit any translational motion. In other words, the substrate is stuck and unable to slide further into or out of the active site. Inspecting the intermolecular interactions in the active site reveals that the cause of this restricted motion is the salt bridge between the fatty acid and Arg241 (see Figure 1b for visualizing the salt bridge). Indeed, this salt bridge was found to be extremely stable throughout the dynamics study. The close superposition of the initial and final structures of the substrate after 25 ns of MD is shown in Figure S5 in the SI document. The salt bridge renders the hydrogen atoms of the β carbon (C_β) completely inaccessible to the Fe-oxo moiety, and thus essentially eliminates the possibility of their undergoing abstraction. By comparison, in $P450_{BS\beta}$ the salt bridge occurs with Arg242, which now provides access to the hydrogen atoms of the β-carbon (C_β), thus leading to β-C−H/α-C−H hydroxylation ratio of 60:40.[6] Further comparative analysis of the active sites of $P450_{BS\beta}$ and $P450_{SP\alpha}$ reveals the former enzyme lacks a residue analogous to Phe288 in its active site. As shown in Figure 1b, in $P450_{SP\alpha}$ this residue is snuggled in between the substrate and heme and thereby it hinders the approach of the β-CH_2 to Fe-oxo. As such, the α-carbon of the substrate is placed close to Fe-oxo group at a distance 2.8 Å while the β carbon is 4.2 Å away from it (see Figure S6). Additionally, due to the steric push of Phe288, the substrate has no room for any conformational changes. In $P450_{BS\beta}$, which lacks a residue analogous to Phe288 between the heme and the substrate, both α and β carbons stay relatively further away (3.5 and 4.8 Å respectively, in Figure S6) from the Fe-oxo group, and there is much more space for substrate dynamics in $P450_{BS\beta}$ than in $P450_{SP\alpha}$. Therefore, these considerations reveal that *the salt bridge and the steric pushing of the substrate's chain by Phe288 create function for the* $P450_{SP\alpha}$ *enzyme and are major factors responsible for the observed regioselectivity of >99% for* α *carbon hydroxylation*. The absence of the steric push in $P450_{BS\beta}$ determines in turn the function in this latter enzyme.

3.3.1. Stereoselectivity in $P450_{SP\alpha}$ *vs Its Pro242Ala Mutant.* Let us turn now to comprehend the enantioselectivity of $P450_{SP\alpha}$. An analysis of the active site reveals that the Pro242 residue exerts a diastereomeric interaction that pushes the *pro-S* C−H closer toward Fe-oxo, as shown in Figure 7. Thus, the substrate adopts a conformation favoring the abstraction of this

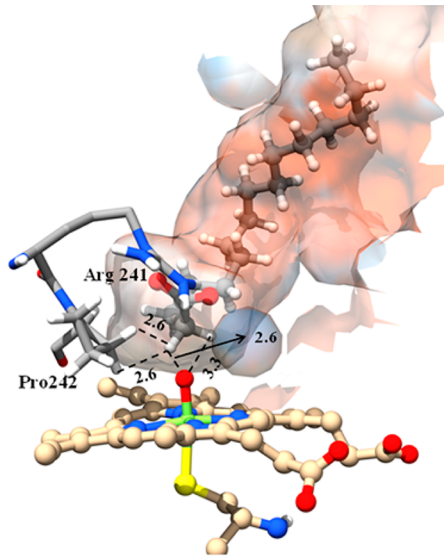

Figure 7. Pro242 and its interaction with the *pro-S* (α-C−H) bond of the substrate. The hydrophobic surface of the substrate channel is shown. Here, dodger blue represents most hydrophilic site and orange reddish shows the most hydrophobic surfaces. Distances are given in Å.

pro-S C−H over the *pro-R* C−H. In order to better elucidate the effect of this steric "push", we have mutated the Pro242 residue with alanine and repeated the simulation for 10 ns. In the Pro242Ala mutant, it is the *pro-R* C−H that stays closer to the Fe-oxo during dynamics. These contrasting results for the wild type (WT) and mutant enzymes confirm that steric induction by Pro242 creates function for the enzyme. It steers the *pro-S* C−H toward the Fe-oxo moiety, and is the major interaction dictating the diastereoselectivity of hydroxylation (see Figure S7 in SI document). Figure 7 shows how this steric induction brings the *pro-S* C−H closer than the *pro-R* C−H (2.6 vs 3.3 Å) to the Fe-oxo moiety of Cpd I. In addition, Figure 7 reveals that the substrate access channel is lined up with hydrophobic residues, providing significantly less room for the substrate's twisting: such rigidity is likely to reinforce the *S*-stereoselectivity induced by Pro242.

To verify the MD predictions in the WT enzyme, we carried out QM/MM optimizations of the diastereomeric transition states for the prochiral HAT, using snapshots from 12 ns into the trajectory, when the *S* and *R* prochiral hydrogen atoms are 2.34 and 3.20 Å, respectively, away from the oxygen atom. The potential energy profiles for the doublet-spin states are displayed in Figure 8 (as shown in Figure S9, the energy profiles for the doublet- and quartet-spin states are close). The optimized transition states have relative energies of 22.4 and 30.9 kcal/mol for **TS2(*S*)** and **TS2(*R*)** with respect to the Cpd I−substrate complex at the QM(B2+ZPE)/MM level of theory.

These calculations reproduce the experimentally observed stereoselectivity and lend support to the MD prediction of a favored juxtaposition of the *pro-S* C−H. Let us then try to understand the root cause of the difference in the barriers. It turns out that, out of the total QM/MM energy difference of 9.7 kcal/mol at the B2 level of theory, the contribution from the QM region to the barrier difference is 4.8 kcal/mol, and the contribution from the MM region is 4.9 kcal/mol. One factor

DOI: 10.1021/jacs.6b01716
J. Am. Chem. Soc. 2016, 138, 6786−6797

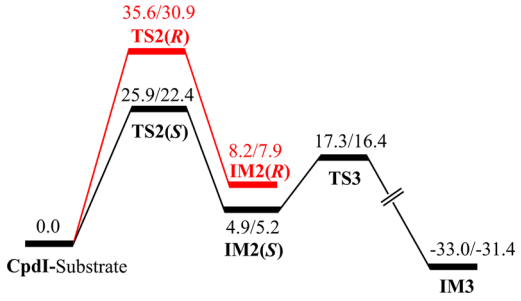

Figure 8. Potential energy profiles for the *R* and *S* hydroxylation reactions at the α carbon atom of the fatty acid. Energies are represented as QM(B2)/MM followed by QM(B2+ZPE)/MM levels of theory in kcal/mol. The red profile is the path not takes. Geometries are named as in Scheme 3.

that surely influences both the QM and MM contributions to this difference in barrier heights is the greater proximity of the *pro-S* C−H to the oxygen atom of the Fe-oxo moiety. One would expect that being close to Fe-oxo, the pro-*S* hydrogen would be abstracted without afflicting significant strain on either the substrate or the enzyme, due to rearrangement required to achieve the transition state. The root cause for the QM contribution to the enantioselectivity can be revealed by a quantitative analysis of the distortion and interaction energies of the respective transition states, **TS2(*S*)** and **TS2(*R*)**, in Figure 9.

Thus, one can generally express the barrier as a sum of the following two components:[31,32]

$$\Delta E^{\ddagger} = \Delta E^{\ddagger}_{\text{dist}} + \Delta E^{\ddagger}_{\text{int}} \quad (1)$$

In the current scenario both diastereomeric transition states originate from the same reactant cluster (Cpd I-Substrate). $\Delta E^{\ddagger}_{\text{dist}}$ is the distortion energy of the reactant fragments, Cpd I and the appended residues of the protein, and the substrate (see Figure 9), in their TS geometries relative to their relaxed geometries at the reactant cluster (Cpd I-Substrate in Figure 7). $\Delta E^{\ddagger}_{\text{int}}$ is the corresponding interaction energy of the two distorted fragments in the TS (see Methods and the SI document, page S9). The TS distortion energies are, 28.4 kcal/mol for **TS2(*R*)** and 24.7 for **TS2(*S*)**. On the other hand, the relative interaction energies are repulsive, +3.9 for **TS2(*R*)** and +2.0 for **TS2(*S*)**, thus essentially conveying that **TS2(*R*)** is more *destabilized* compared to **TS2(*S*)**. In summary, therefore, **TS2(*S*)** is favored over **TS2(*R*)** in terms of both distortion and interaction energies.

The more demanding geometric changes required to abstract the *R* prochiral hydrogen are visible in Figure 9, for **TS2(*R*)** compared to **TS2(*S*)**. The hydrogen bond (H2−O2) of the salt bridge in **TS2(*R*)** is elongated to 1.73 Å vs. 1.64 Å in **TS2(*S*)**. In addition, the **TS2(*R*)** transition state has a more eclipsed $CC_{\alpha}C_{\beta}C_{\gamma}$ dihedral angle of 24.6° than **TS2(*S*)** wherein dihedral angle is 57.2°. All these factors taken together raise the energy of **TS2(*R*)** vs **TS2(*S*)**.

Searching for the causes of the higher MM contribution to the barrier for *R*-hydroxylation, we found that the formation of **TS2(*R*)** increases the substrate-Pro242 repulsive interactions. Thus, a superposition of the both diasteromeric transition states given in Figure S8 of the SI document reveals that in **TS2(*R*)** the α-carbon atom of the substrate is only 2.8 Å away from Pro242, whereas in **TS2(*S*)** the distance is 3.2 Å away. It follows, therefore, that the active site of $P450_{SP\alpha}$ and specifically its Pro242 residue play the major role in *destabilizing* the *pro-R* transition state relative to the *pro-S* one, and in inflicting greater distortion energy for abstraction of the *pro-R* C−H atom compared with the *pro-S* C−H. *These decisive effects (4.8 kcal/mol in the QM and the rest in the MM), are sufficient to render an enantiomeric excess larger than 90%, and endow* $P450_{SP\alpha}$ *with enantioselective function.*

So far, we have shown the reactivity on the doublet-spin state, and one may wonder what about the ubiquitous *two state reactivity (TSR)*[1h,35] due to the virtually degenerate doublet- and quartet- spin states of Cpd I?[1] This was tested and the TSR mechanism was ascertained. Indeed, here too, the quartet spin state lies only 0.5 kcal/mol above the doublet state, while in the

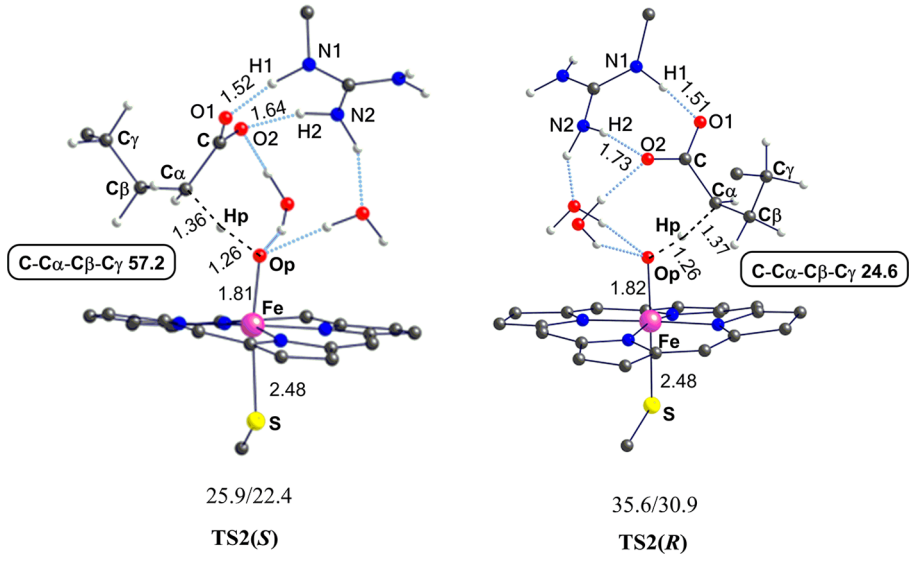

Figure 9. QM(B1)/MM Optimized geometries of H-abstraction transition states, **TS2(*S*)** and **TS2(*R*)**. The Relative energies vis-à-vis the reactant cluster are indicated below the structures at the QM(B2)/MM followed by QM(B2+ZPE)/MM levels of theory. Distances are given in Å and angles are in degrees. The fragments used for the energy component analysis are the fatty acid substrate (Fragment 1) and the rest of molecules (Fragment 2).

DOI: 10.1021/jacs.6b01716
J. Am. Chem. Soc. 2016, 138, 6786−6797

H-abstraction TS the energy difference is 1.0 kcal/mol, similar to earlier findings (the TSR energy profile is shown in Figure S9 in the SI). Since the HAT is the rate-determining step, and since the radical produced by HAT is locked in position, the final chirality is unaffected by the rebound barriers, such that TSR has no consequences on the final chemical outcome.

3.4. Comparison of $P450_{SP\alpha}$ to $P450_{BM3}$ and to $P450_{BS\beta}$. $P450_{BM3}$ is another fatty acid hydroxylase that performs regio- and enantioselective hydroxylation of fatty acids, but very differently than $P450_{SP\alpha}$.[5] Thus, $P450_{BM3}$ hydroxylates the fatty acid at the C-terminal (at the ω-1, ω-2 and ω-3 CH_2 sites) of the fatty acid instead of carboxylic terminal as done by $P450_{SP\alpha}$. Both enzymes are stereoselective hydoxylases. What are the minimal factors that make these two fatty acid hydroxylases function differently?

On the basis of our previous study[5c] and the present one, the major factor that determines the function of $P450_{BM3}$ vis-à-vis $P450_{SP\alpha}$ is the different mode of substrate binding as shown in Figure 10. Thus, in $P450_{BM3}$, the fatty acid head is bound by

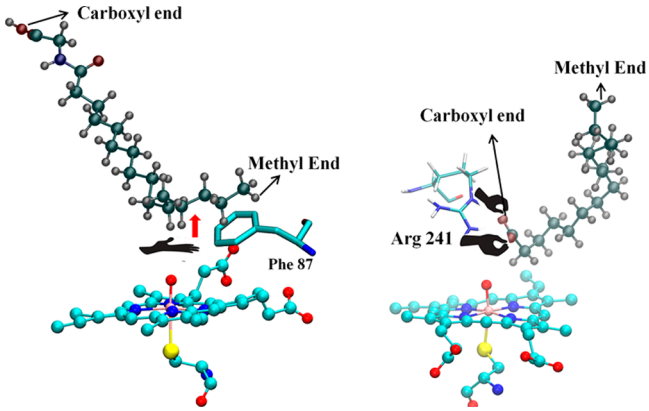

Figure 10. Modes of binding of fatty acids in $P450_{BM3}$ (left) and in $P450_{SP\alpha}$ (right). The CH_2 sites ω-1, ω-2 and ω-3 are accessible for hydroxylation in $P450_{BM3}$.

Arg47 and Tyr51, which reside at the opening of the substrate channel, near the protein surface. Consequently, the substrate's C-tail goes into the inside of the active site near the heme. The free movement of the C-tail, within the active site, requires conformational assistance by Phe87 which resides near the heme and causes the C-tail to curl and expose its nonterminal CH_2 positions (ω-1/ω-2/ω-3) to Cpd I.[5c] By contrast, in the active site of the $P450_{SP\alpha}$ enzyme, the fatty acid is held by its carboxylate head through a salt bridge with Arg241. As such, this bonding mode sequesters the α-CH_2 group of the fatty acid in proximity to Cpd I leading to a regioselective α-hydroxylation. By comparison, in $P450_{BS\beta}$ the salt bridge occurs with Arg242 and thereby provides access to the hydrogen atoms of the β-carbon (C_β), thus leading to preference of β-C−H hydroxylation. The $P450_{BS\beta}$ enzyme further lacks the steric push from Phe288 as compared to $P450_{SP\alpha}$. These observations highlight the uniqueness of each class of enzymes. In $P450_{BM3}$, Phe87-controlls the dynamics of the fatty acid tail inside active site and determines the regioselectivity, while in $P450_{SP\alpha}$ and in $P450_{BS\beta}$, the extent of sequestering of the fatty acid by its head leads to the reported regioselectivity. The enantioselectivity may be a byproduct of this sequestering.

Furthermore, in the absence of Arginine near the heme in $P450_{BM3}$, the formation of Cpd I follows the native catalytic cycle, with reductive activation of molecular oxygen, whereas due to the presence of the carboxylate head of the substrate, the Arg241/Arg242 and two crystal waters near the heme in $P450_{SP\alpha}$/$P450_{BS\beta}$, the native process of these enzymes is the creation of Cpd I via H_2O_2. *Evidently, very few residues and crystal waters are necessary to create different functions for these related P450 hydroxylases.*

4. CONCLUSIONS

Combined QM/MM and MD simulations revealed the following mechanistic aspects of H_2O_2 dependent hydroxylations of fatty acids by the $P450_{SP\alpha}$ enzyme.

As in other P450s studied,[10a] when H_2O_2 is the surrogate oxidant, Cpd I's generation in $P450_{SP\alpha}$ follows an "*effectively concerted nonsynchronous*" mechanism, whereby H_2O_2 dissociates homolytically in the active site of the enzyme, while the HO· radical, which is sequestered by Arg241, the substrate's carboxylate head, and two crystal waters, can only abstract the hydrogen from the ferric-hydroxo moiety to generate Cpd I. *What creates this function is the fatty acid binding by Arg241, which stabilizes the Fe(III)-H_2O_2 complex.* Our results show that the generation of Cpd 0 (Fe(III)-OOH) through "substrate assisted catalysis" is a high energy and hence an inefficient process and not feasible.

The regio- and stereoselectivity of hydroxylation in $P450_{SP\alpha}$ are due to the fatty acid binding by Arg241 and the nearby Pro242 residue, which controls the movements of the two C−H bonds of the α-CH_2 group of the fatty acid. Thus, Arg241 forms a salt bridge to the substrate's carboxylate head, and this causes proximity between the α-CH_2 group and Cpd I, thereby leading to exclusive α-hydroxylation. This regioselectivity is further assisted by the steric factors induced by Phe288 in the active site. At the same time, Pro242 makes the selection between the two α-hydrogens, by pushing the *pro-S* C−H toward the Fe-oxo group of Cpd I, while hydrophobic interactions with the substrate channel create a rigid active site that prevents the substrate's twisting. These cumulative *diastereomeric interactions* lead to the oxidation of only the *pro-S* C−H bond. The function of Pro242 is further confirmed by an MD simulation with a Pro242Ala mutant enzyme, which brings the *pro-R* C−H bond closer to the Fe-oxo group.

QM/MM calculations of the HAT barriers reveal the exclusive *pro-S* selectivity. Comparing the two transition states, we find that the *pro-R* transition state distorts more than the *pro-S* transition state, due to partial disruption of the salt bridge with Arg241, and to excessive repulsive interaction of the *pro-S* C−H with Pro242 in the *pro-R* transition state. These factors create a much higher barrier for the pro-*R* transition state and prefer the *pro-S* C−H activation. It is apparent therefore that the enzyme penalizes reactions of improperly juxtaposed moieties of the substrates.

Finally, comparison of $P450_{SP\alpha}$ to the other fatty acid hydroxylases, $P450_{BM3}$ and $P450_{BS\beta}$, shows that in each case very few residues are required to create specific function. *This minimal requirement for "function" accounts for the huge versatility of the P450 superfamily.*

■ ASSOCIATED CONTENT

Supporting Information

The Supporting Information is available free of charge on the ACS Publications website at DOI: 10.1021/jacs.6b01716.

DOI: 10.1021/jacs.6b01716
J. Am. Chem. Soc. 2016, 138, 6786−6797

Potential energy profiles, graphical representation of simulation trajectory, orbital pictures, optimized geometries, (Figure S1−S9) Mulliken spin and charges (Table S1−S4), Full citation of Gaussian 09, Details of distortion/interaction analysis, absolute QM/MM energies and Cartesian coordinates of the optimized QM region of stationary points. (PDF)

AUTHOR INFORMATION

Corresponding Author

*sason@yfaat.ch.huji.ac.il

Notes

The authors declare no competing financial interest.

ACKNOWLEDGMENTS

SS is supported by the Israel Science Foundation (ISF grant 1183/13). RR, KDD and BW acknowledge the Planning and Budgeting Committee (PBC) of the council for higher education in Israel for the Post Doctoral Fellowships. Dina A. Sharon is thanked for useful discussions. The paper is dedicated to W. L. Jorgensen.

REFERENCES

(1) (a) Groves, J. T. *J. Chem. Educ.* **1985**, *62*, 928−931. (b) Gerber, N. C.; Sligar, S. G. *J. Biol. Chem.* **1994**, *269*, 4260−4266. (c) Sono, M.; Roach, M. P.; Coulter, E. D.; Dawson, J. H. *Chem. Rev.* **1996**, *96*, 2841−2887. (d) Vidakovic, M.; Sligar, S. G.; Li, H.; Poulos, T. L. *Biochemistry* **1998**, *37*, 9211−9219. (e) Ortiz de Montellano, P. R. *Cytochrome P450: Structure, Mechanism, and Biochemistry*, 3rd ed.; Kluwer Academic/Plenum Publishers: New York, 2005. (f) van Eldik, R. *Chem. Rev.* **2005**, *105*, 1917−2722. (g) Denisov, I. G.; Makris, T. M.; Sligar, S. G.; Schlichting, I. *Chem. Rev.* **2005**, *105*, 2253−2277. (h) Shaik, S.; Cohen, S.; Wang, Y.; Chen, H.; Kumar, D.; Thiel, W. *Chem. Rev.* **2010**, *110*, 949−1017. (i) Rittle, J.; Green, M. T. *Science* **2010**, *330*, 933−937. (j) Groves, J. T. *Nat. Chem.* **2014**, *6*, 89−91. (k) Mak, P. J.; Luthra, A.; Sligar, S. G.; Kincaid, J. R. *J. Am. Chem. Soc.* **2014**, *136*, 4825−4828.

(2) (a) Martinis, S. A.; Atkins, W. M.; Stayton, P. S.; Sligar, S. G. *J. Am. Chem. Soc.* **1989**, *111*, 9252−9253. (b) Joo, H.; Lin, Z.; Arnold, F. H. *Nature* **1999**, *399*, 670−673. (c) Koo, L. S.; Tschirret-Guth, R. A.; Straub, W. E.; Moenne-Loccoz, P.; Loehr, T. M.; de Montellano, P. R. O. *J. Biol. Chem.* **2000**, *275*, 14112−14123.

(3) Matsunaga, I.; Kusunose, E.; Yano, I.; Ichihara, K. *Biochem. Biophys. Res. Commun.* **1994**, *201*, 1554−1560.

(4) (a) Matsunaga, I.; Yamada, M.; Kusunose, E.; Nishiuchi, Y.; Yano, I.; Ichihara, K. *FEBS Lett.* **1996**, *386*, 252−254. (b) Stumpf, P. K. *J. Biol. Chem.* **1956**, *223*, 643−649.

(5) (a) Volz, T. J.; Rock, D. A.; Jones, J. P. *J. Am. Chem. Soc.* **2002**, *124*, 9724−9725. (b) Cryle, M. J.; De Voss, J. J. *Angew. Chem., Int. Ed.* **2006**, *45*, 8221−8223. (c) Dubey, K. D.; Wang, B.; Shaik, S. *J. Am. Chem. Soc.* **2016**, *138*, 837−845.

(6) Lee, D. S.; Yamada, A.; Sugimoto, H.; Matsunaga, I.; Ogura, H.; Ichihara, K.; Adachi, S.; Park, S. Y.; Shiro, Y. *J. Biol. Chem.* **2003**, *278*, 9761−9767.

(7) Shoji, O.; Fujishiro, T.; Nakajima, H.; Kim, M.; Nagano, S.; Shiro, Y.; Watanabe, Y. *Angew. Chem., Int. Ed.* **2007**, *46*, 3656−3659.

(8) Fujishiro, T.; Shoji, O.; Nagano, S.; Sugimoto, H.; Shiro, Y.; Watanabe, Y. *J. Biol. Chem.* **2011**, *286*, 29941−29950.

(9) (a) Poulos, T. L. *Chem. Rev.* **2014**, *114*, 3919−3962. (b) Lai, W.; Chen, H.; Matsui, T.; Omori, K.; Unno, M.; Ikeda-Saito, M.; Shaik, S. *J. Am. Chem. Soc.* **2010**, *132*, 12960−12970.

(10) (a) Cho, K. B.; Derat, E.; Shaik, S. *J. Am. Chem. Soc.* **2007**, *129*, 3182−3188. (b) Chen, H.; Moreau, Y.; Derat, E.; Shaik, S. *J. Am. Chem. Soc.* **2008**, *130*, 1953−1965. (c) Wang, B.; Li, C.; Dubey, K. D.; Shaik, S. *J. Am. Chem. Soc.* **2015**, *137*, 7379−7390.

(11) Sicking, W.; Korth, H.-G.; Jansen, G.; de Groot, H.; Sustmann, R. *Chem. - Eur. J.* **2007**, *13*, 4230−4245.

(12) Olsson, M. H.; Søndergard, C. R.; Rostkowski, M.; Jensen, J. H. *J. Chem. Theory Comput.* **2011**, *7*, 525−537.

(13) Jorgensen, W. L.; Chandrasekhar, J.; Madura, J. D.; Impey, R. W.; Klein, M. L. *J. Chem. Phys.* **1983**, *79*, 926−935.

(14) Humphrey, W.; Dalke, A.; Schulten, K. *J. Mol. Graphics* **1996**, *14*, 33−38.

(15) (a) Zheng, J.; Altun, A.; Thiel, W. *J. Comput. Chem.* **2007**, *28*, 2147−2158. (b) Senn, H. M.; Thiel, W. *Top. Curr. Chem.* **2007**, *268*, 173−290. Other QM/MM approaches are described in (c) Ryde, U. *Curr. Opin. Chem. Biol.* **2003**, *7*, 136−142. (d) Lin, H.; Truhlar, D. G. *Theor. Chem. Acc.* **2007**, *117*, 185−199. (e) Olah, J.; Mulholland, A. J.; Harvey, J. N. *Proc. Natl. Acad. Sci. U. S. A.* **2011**, *108*, 6050−6055. (f) Chung, L. W.; Sameera, W. M. C.; Ramozzi, R.; Page, A. J.; Hatanaka, M.; Petrova, G. P.; Harris, T. V.; Li, X.; Ke, Z.; Li, H.; Ding, L.; Morokuma, K. *Chem. Rev.* **2015**, *115*, 5678−5796.

(16) Izaguirre, J. A.; Catarello, D. P.; Wozniak, J. M.; Skeel, R. D. *J. Chem. Phys.* **2001**, *114*, 2090−2098.

(17) Brooks, B. R.; Brooks, C. L., III; MacKerell, A. D., Jr.; Nilsson, L.; Petrella, R. J.; Roux, B.; Won, Y.; Archontis, G.; Bartels, C.; Boresch, S.; Caflisch, A.; Caves, L.; Cui, Q.; Dinner, A. R.; Feig, M.; Fischer, S.; Gao, J.; Hodoscek, M.; Im, W.; Kuczera, K.; Lazaridis, T.; Ma, J.; Ovchinnikov, V.; Paci, E.; Pastor, R. W.; Post, C. B.; Pu, J. Z.; Schaefer, M.; Tidor, B.; Venable, R. M.; Woodcock, H. L.; Wu, X.; Yang, W.; York, D. M.; Karplus, M. *J. Comput. Chem.* **2009**, *30*, 1545−1614.

(18) Vidossich, P.; Fiorin, G.; Alfonso-Prieto, M.; Derat, E.; Shaik, S.; Rovira, C. *J. Phys. Chem. B* **2010**, *114*, 5161−5169.

(19) Phillips, J. C.; Braun, R.; Wang, W.; Gumbart, J.; Tajkhorshid, E.; Villa, E.; Chipot, C.; Skeel, R. D.; Kalé, L.; Schulten, K. *J. Comput. Chem.* **2005**, *26*, 1781−1802.

(20) (a) Sherwood, P.; de Vries, A. H.; Guest, M. F.; Schreckenbach, G.; Catlow, C. R. A.; French, S. A.; Sokol, A. A.; Bromley, S. T.; Thiel, W.; Turner, A. J.; Billeter, S.; Terstegen, F.; Thiel, S.; Kendrick, J.; Rogers, S. C.; Casci, J.; Watson, M.; King, F.; Karlsen, E.; Sjovoll, M.; Fahmi, A.; Schäfer, A.; Lennartz, C. *J. Mol. Struct.: THEOCHEM* **2003**, *632*, 1−28. (b) Metz, S.; Kästner, J.; Sokol, A.; Keal, T.; Sherwood, P. *WIREs Comput. Mol. Sci.* **2014**, *4*, 101−110.

(21) Ahlrichs, R.; Bär, M.; Häser, M.; Horn, H.; Kölmel, C. *Chem. Phys. Lett.* **1989**, *162*, 165−169.

(22) Smith, W.; Forester, T. R. *J. Mol. Graphics* **1996**, *4*, 136−141.

(23) Bakowies, D.; Thiel, W. *J. Phys. Chem.* **1996**, *100*, 10580−10594.

(24) Becke, A. D. *J. Chem. Phys.* **1993**, *98*, 5648−5652.

(25) Altun, A.; Breidung, J.; Neese, F.; Thiel, W. *J. Chem. Theory Comput.* **2014**, *10*, 3807−3820.

(26) (a) Hehre, W. J.; Ditchfield, R.; Pople, J. A. *J. Chem. Phys.* **1972**, *56*, 2257−2261. (b) Francl, M. M.; Petro, W. J.; Hehre, W. J.; Binkley, J. S.; Gordon, M. S.; De Frees, D. J.; Pople, J. A. *J. Chem. Phys.* **1982**, *77*, 3654−3665. (c) Clark, T.; Chandrasekhar, J.; Spitznagel, G. W.; Schleyer, P. v. R. *J. Comput. Chem.* **1983**, *4*, 294−301. (d) Hay, P. J.; Wadt, W. R. *J. Chem. Phys.* **1985**, *82*, 299−310.

(27) Weigend, F.; Ahlrichs, R. *Phys. Chem. Chem. Phys.* **2005**, *7*, 3297−3305.

(28) Billeter, S. R.; Turner, A. J.; Thiel, W. *Phys. Chem. Chem. Phys.* **2000**, *2*, 2177−2186.

(29) Some transition states are difficult to optimize in QM/MM calculations. In such cases the barrier can be derived from the relaxed potential energy scan. See the reference: Sen, K.; Thiel, W. *J. Phys. Chem. B* **2014**, *118*, 2810−2820.

(30) Frisch, M. J. et al. *Gaussian 09*, revision D.01; Gaussian, Inc.: Pittsburgh, PA, 2009. Full citations are available in Supporting Information.

(31) For development of the method, see the following: (a) Morokuma, K. J. *J. Chem. Phys.* **1971**, *55*, 1236−1244. (b) Kitaura, K.; Morokuma, K. *Int. J. Quantum Chem.* **1976**, *10*, 325−340. (c) Ziegler, T.; Rauk, A. *Theor. Chim. Acta.* **1977**, *46*, 1−10. (d) Ziegler, T.; Rauk, A. *Inorg. Chem.* **1979**, *18*, 1558−1565. For usage of the terms distortion/deformation energies, see the following:

DOI: 10.1021/jacs.6b01716
J. Am. Chem. Soc. 2016, 138, 6786−6797

(e) Strozier, R. W.; Caramella, P.; Houk, K. N. *J. Am. Chem. Soc.* **1979**, *101*, 1340−1343. (f) Mitchell, D. J.; Schlegel, H. B.; Shaik, S.; Wolfe, S. *Can. J. Chem.* **1985**, *63*, 1642−1649. (g) Guthrie, J. P. *ChemPhysChem* **2003**, *4*, 809−816. (h) Ess, D. H.; Houk, K. N. *J. Am. Chem. Soc.* **2007**, *129*, 10646−10647. (i) Legault, C. Y.; Garcia, Y.; Merlic, C. A.; Houk, K. N. *J. Am. Chem. Soc.* **2007**, *129*, 12664−12665. (j) Ess, D. H.; Houk, K. N. *J. Am. Chem. Soc.* **2008**, *130*, 10187−10198. (k) Rajeev, R.; Sunoj, R. B. *J. Org. Chem.* **2013**, *78*, 7023−7029.

(32) For applications to reactivity, see the following: (a) van Zeist, W.-J.; Bickelhaupt, F. M. *Org. Biomol. Chem.* **2010**, *8*, 3118−3127. (b) Diefenbach, A.; Bickelhaupt, F. M. *J. Phys. Chem. A* **2004**, *108*, 8460−8466.

(33) Wang, B.; Li, C.; Cho, K. B.; Nam, W.; Shaik, S. *J. Chem. Theory Comput.* **2013**, *9*, 2519−2525.

(34) Derat, E.; Shaik, S.; Rovira, C.; Vidossich, P.; Alfonso-Prieto, M. *J. Am. Chem. Soc.* **2007**, *129*, 6346−6347.

(35) (a) Shaik, S.; Kumar, D.; de Visser, S. P.; Altun, A.; Thiel, W. *Chem. Rev.* **2005**, *105*, 2279−2328. (b) Meunier, B.; de Visser, S. P.; Shaik, S. *Chem. Rev.* **2004**, *104*, 3947−3980.

DOI: 10.1021/jacs.6b01716
J. Am. Chem. Soc. 2016, 138, 6786−6797